SUPPLEMENTAL MATERIALS

I. SUPPLEMENTAL METHODS

1. Study cohorts

We studied five unrelated Japanese SQTS families consisting of 10 affected members. The QT interval was corrected for heart rate using Bazett's equation ($QTc=QT/(\sqrt{RR})$). The diagnosis of SQTS was made based on QTc ≤ 330 ms or QTc < 360 ms with presence of VF episode, pathogenic mutations, or family history of SQTS or SCD before age of 40 years [1]. All individuals who participated in the study gave written informed consent prior to genetic and clinical investigations in accordance with the standards of the Declaration of Helsinki and the local ethics committees at each participating institution. To further characterize the genotype-specific characteristics, we created an additional cohort, which consisted of 132 SQTS patients (80 men and 52 women; age of manifestation: 25 ± 19 years) including five families (10 cases) from the current study, 33 families (61 cases) from a review by Gollob et al [2], and an additional 36 SQTS families (61 cases) that have been previously reported and available on PubMed as of May 2014 [2-18]. (Supplemental Table S1)

2. Genetic analysis

Genomic DNA was extracted from the blood using Gentra Puregene Blood Kit (Qiagen, Venlo, Netherland). All the exons of *KCNH2*, *KCNQ1*, and *KCNJ2* were PCR amplified as previously described [19-21]. The primer sequences for *KCNJ2* are available in the supplemental Table S2. In some cases, additional genetic screenings were performed for mutations in Brugada syndrome candidate genes, including *SCN5A*, *HCN4*, *KCND3*, *KCNE3*, *SCN1B*, *SCN3B*, *SCN10A*, and *TRPM4* [22-28]. Direct sequencing was performed using the ABI Genetic Analyzer 3130 (Life Technologies, Carlsbad, CA) and results were verified against a control group of 200 healthy subjects and publicly available variation databases including dbSNP, 1,000 Genomes project, Exome Variant

Server, and Human Genetic Variation Database (HGVD, exome sequencing data of 1,208 Japanese individuals, http://www.genome.med.kyoto-u.ac.jp/SnpDB/).

3. Biophysical analysis of *KCNH2*-I560T

Site-directed mutagenesis was performed using the QuikChange site-directed mutagenesis kit (Agilent Technologies, Santa Clara CA) on human *KCNH2* cDNA (a gift from Gail Robertson, University of Wisconsin) cloned in an expression plasmid pcDNA3.1. (Life Technologies) Oligonucleotide sequences are available in supplemental Table S2. Plasmids were then sequenced to verify creation of the mutation and to exclude polymerase errors. The COS-7 cell lines were transiently transfected with wild-type (WT) or I560T *KCNH2* plasmid (1.5 μg) together with pEGFP-C1 (0.5 μg) (Takara Bio Inc., Otsu, Japan) using Lipofectamine LTX. (Life Technologies) Twenty-four hours after transfection, the potassium current were recorded from the cells by whole-cell patch-clamp techniques at 2 kHz with a low pass filter set to 1 kHz using Axopatch 200B (Molecular Devices, Sunnyvale, CA) and pClamp 8 software (Molecular Devices). Holding potential was -90 mV. The cells were superfused with normal Tyrode (in mmol/L) (NaCl 145, KCl 4, $CaCl_2$ 1.8, $MgCl_2$ 1, HEPES 10, glucose 10, pH=7.35) at 37 °C. The micropipette had resistance of 3-4 MΩ when filled with a pipette solution containing (in mmol/L) K-asparate 100, Na_2-creatine phosphate 5, KCl 30, MgATP 5, EGTA 3, HEPES 5 (pH=7.2).

Current-voltage relationship and voltage-dependent activation were determined by test pulses from -40 mV to 40 mV in 10 mV steps for 4 sec followed by a pulse of -60 mV, and peak potassium current for WT and I560T mutant *KCNH2* channel were measured. Steady-state inactivation was measured with three-pulse protocol consisting of a +40 mV depolarizing pulse for 2 sec, then followed by a voltage array from -100 mV to +80 mV, followed by a test pulse at +40 mV. The current-voltage relationship was obtained by normalized peak tail current amplitude at each test pulse in 10 mV steps. Voltage-dependence of activation and steady-state inactivation data were fitted to the Boltzmann equation: $I/Imax = [1 + \exp((V_{1/2} - V)/k)]^{-1}$ to determine the membrane potential for half maximal inactivation ($V_{1/2}$) and the slope factor k [3]. Data were analyzed using Clampfit 10 (Molecular Devices) and SigmaPlot11.2 (SYSTAT software, San Jose, CA).

4. Western blotting

The novel SQTS mutation *KCNH2*-I560T is neighboring an LQTS mutation A561V [29], which is characterized by its trafficking instability resulting in a loss of channel function. To test if the I560T mutant channel has trafficking abnormalities, HeLa cells were transfected with 0.5 μg of *KCNH2* plasmid of either WT, I560T, or A561V using Lipofectamine LTX. Forty-eight hours after transfection, cells were harvested and protein was extracted by a lysis buffer (1% Nonidet-P40, 1 mM EDTA, 150 mM NaCl,

10 mM Tris-HCl, pH=7.8) supplemented with 25x Complete lysis solution (Roche Applied Science, Penzburg, Germany) at 4° C. Protein concentration was determined using BCA Protein Assay Reagent kit. (Pierce, Rockford, IL) Thirty micrograms cellular extracts were separated on sodium dodecyl sulfate polyacrylamide gel electrophoresis gel and transferred to polyvinyl difluoride membranes. After blocking with 5% skim milk in phosphate buffered saline (PBS) for one hour, membranes were incubated overnight at 4° C with primary anti-*KCNH2* polyclonal antibodies (1:400, Life Technologies) for *KCNH2* staining. Membranes were also incubated with primary anti-β actin polyclonal antibodies (1:200, Cell Signaling Technology, Danvers, MA) for overnight at 4° C. After three washes with PBS + 0.1% Tween-20, both membranes were also incubated with anti-rabbit IgG horseradish peroxidase-conjugated second antibodies (1:1000, GE Healthcare, Little Chalfont, UK) for one hour at 37° C. After washing with PBS + 0.1% Tween-20, signals were visualized by ECL Prime Detection Reagent (GE Healthcare) and Imager Fluorchem FC2 (Cell BioSciences, Santa Clara, CA).

5. Computer simulation of action potential shortening and abbreviated QTc in 1-D model

Through *in silico* methods, we can determine the tissue level electrophysiology by using the *in vitro* experimental data of a given mutation's ion channel kinetics. O'Hara-Rudy dynamic is a ventricular cell model based on experimental undiseased human ventricular cell data [30]. By using this model, we are able to calculate the action potential duration and simulate ECG for WT and *KCNH2*-I560T on a human level. This process can evaluate whether the relatively small shift of I560T shift inactivation in the absence of activation properties can cause the clinically observed shortened QT interval in our patient.

To elucidate the effects of the *KCNH2*-I560T mutation on the human ventricular action potentials, we conducted simulations of paced propagation in a 0.9 cm bidomain myofiber with transverse conductivity, mimicking transmural section of left ventricular free wall consisting of 0.06 cm endocardial, 0.6 cm midmyocardial, and 0.24 cm epicardial layers [31]. Membrane kinetics were basically represented by the O'Hara-Rudy dynamic human ventricular model [30]. To adjust the conduction velocity of the excitation wavefront, maximum conductance of the original fast I_{Na} was multiplied 3-fold, which did not change the action potential form of repolarization phases. Furthermore, the original I_{Kr} was replaced by the following Markovian I_{Kr} (μA/μF) with WT or I560T mutation based on our experimental data:

$$I_{Kr} = G_{Kr} \times P_O \times (V_m - E_K),$$

where G_{Kr} (mS/μF) is the maximum conductance of I_{Kr}; P_O is the open probability of I_{Kr}; V_m (mV) is the membrane potential; and E_K (mV) is the reversal potential for K^+. The G_{Kr} values for *KCNH2*-WT and *KCNH2*-I560T mutation are given by:

For WT, $G_{Kr} = 0.0243 \times [K^+]_o^{0.59}$

For I560T, $G_{Kr} = 0.035235 \times [K^+]_o^{0.59}$

where $[K^+]_o$ is the extracellular potassium concentration. The Markovian I_{Kr}, of which basic structure was originally reported by Clancy and Rudy [32], includes an open state (O), an inactivation state (I), and 3 closed states (C1, C2, and C3). Between each state is a forward and backward transition rates. Forward: $\alpha=\alpha_0 \times \exp(Z_\alpha \times V\text{m}/(\text{RT/F}))$ Backward: $\beta=\beta_0 \times \exp(-Z_\beta \times V\text{m}/(\text{RT/F}))$, α_0, β_0 = rate coefficient at V_m= 0 V, Vm = transmembrane voltage, Z=equivalent valence, R= universal gas constant, T= absolute temperature, F=Faraday's constant.

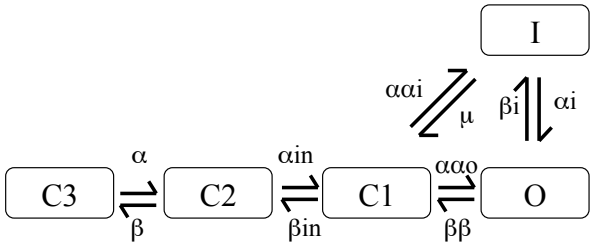

The basic Clancy-Rudy structure was used with modified transition rates in accordance to our experimental data or transition rates reported by Adeniran et al [33]. In the present study, the transition rates between the states in cases of WT and I560T mutation are given by the following formulations:

For both WT and I560T,

C1→O or C1→I	$\alpha\alpha_o = \alpha\alpha_i = 0.00655 \times \exp(0.027735765 \times (V_m - 46))$
C2→C1	$\alpha_{in} = 2.172$
C2←C1	$\beta_{in} = 1.077$
C3→C2	$\alpha = 0.001332 \times \exp(0.05547153 \times (V_m - 12))$
C3←C2	$\beta = 0.002357 \times \exp(-0.036588 \times V_m)$
O←I	$\alpha_i = 0.4829 \times \exp(-0.029988 \times (V_m + 60)) \times (4.5 / [K^+]_o)$
C1←I	$\mu = (\alpha_i \times \beta\beta \times \alpha\alpha_i) / (\alpha\alpha_o \times \beta_i)$

For WT,

C1←O	$\beta\beta = 0.00117428 \times \exp(-0.0148902 \times V_m)$
O→I	$\beta_i = 0.2624 \times \exp(0.0007065 \times (V_m + 35)) \times (4.5 / [K^+]_o)^{0.3}$

For I560T,

C1←O	$\beta\beta = 0.5 \times 0.001178428 \times \exp(-0.0148902 \times V_m)$
O→I	$\beta_i = 0.5 \times 0.2624 \times \exp(0.0007065 \times (V_m + 35)) \times (4.5 / [K^+]_o)^{0.3}$

The time discretization and spatial discretization were 5 μs and 7.5 μm, respectively. The extracellular and intracellular tissue conductivities (g_{et} and g_{it}) were 2.36 mS/cm and 0.38 mS/cm, respectively, except that epicardial g_{it} was decreased by 34% [34]. Pacing stimuli of 2 ms and strength twice-diastolic threshold were applied

transmembranously to the endocardial end at a cycle length of 1,000 ms. To get ECG similar to the left precordial ECG, a unipolar recording electrode was located 2 cm above the epicardial end of the tissue. The method for calculating ECG was described elsewhere [35].

6. Computer simulation of VF inducibility in *KCNH2*-I560T

To demonstrate the relative arrhythmogenicity of *KCNH2*-I560T mutation, we additionally conducted simulations of VF in the bidomain endocardial sheet in the presence or absence of the mutation. The model consisted of a homogeneous and isotropic bidomain endocardial myocardial sheet 3×3 cm (90,000 discrete myocardial units). The time discretization and spatial discretization were 5 μs and 10 μm, respectively. The extracellular and intracellular tissue conductivities were 4.305 mS/cm and 0.965 mS/cm, respectively. As a model of VF, a spiral wave reentry was induced by an S1-S2 cross-field protocol [36]. The ECG was simulated as being recorded by a unipolar electrode located 2 cm above the center of the myocardial sheet.

7. Comparison of clinical characteristics of genotyped SQTS patients

PubMed database was searched for SQTS relevant English publications before May 2014. In study cohort of 132 patients, 65 patients were genotype-positive (6 from the current study and 59 from previous reports [2-13]) of whom 30 (46%) were male and had a mean age of manifestation of 28 ± 20 years (ranging from 0 and 72). SQTS patients had causative mutations in *KCNH2* (SQT1; n=34), *KCNQ1* (SQT2; n=8), *KCNJ2* (SQT3; n=9), *CACNA1C* (SQT4; n=5), *CACNB2* (SQT5; n=6), and *CACNA2D1* (SQT6; n=3) (Supplemental table S1). Available clinical variables for each reported patient were extracted for sex, age of manifestation, QT, QTc, heart rate, causative gene and mutation, and clinical history: AF, SCD/aborted cardiac arrest, palpitations/syncope, and SSS/bradycardia. Bradycardia for adult patients was evaluated based on heart rate < 50 bpm. For children, bradycardia was determined based on heart rate < 100 bpm for ages 0 to 3 years and on heart rate<60 bpm for ages 3-9 years [37]. A patient was considered symptomatic in the presence of the before mentioned clinical episodes. Age of manifestation and QTc values were compared among SQT1, SQT2, and SQT3-6. Due to limited number of SQTS patients, other clinical variables were compared between genotype-specific subgroups and the remainder of SQTS genotype-positive patients; SQT1 vs non-SQT1 and SQT2 vs non-SQT2.

8. Statistical analysis

Data are reported as mean ± SD and analyzed by one-way ANOVA with Bonferroni post-hoc analysis using JMP10 (JMP, Cary, NC). The univariate clinical variables are presented as percentages, and analyzed by χ^2-test or Fisher extract test. Statistical significance was set at $P<0.05$.

II. SUPPLEMENTAL TABLES

Table S1: Numbers of patients included in two SQTS cohorts

Patients (probands)	Mutation-positive							Non-genotyped	Total
	SQT1	SQT2	SQT3	SQT4	SQT5	SQT6	SQT1-6		
Current study	4 (2)	2 (1)	0	0	0	0	6 (3)	4 (2)	10 (5)
Previous studies	30 (14)	6 (6)	9 (7)	5 (3)	6 (1)	3 (1)	59 (32)	63 (37)	122 (69)
Total	34 (16)	8 (7)	9 (7)	5 (3)	6 (1)	3 (1)	65 (35)	67 (39)	132 (74)

(Probands: shown with parentheses)

Table S2: Sequences of PCR and site-directed mutagenesis primers

Name	Sequence (5' to 3')
KCNJ2-Exon2-F	AAACTGTTTCTCCAAAGCGTT
KCNJ2-Exon2-R	CAACATCTATGTGCCATCGG
KCNH2-I560T-F	ACCTTTGCGCTCACCGCGCACTGGC
KCNH2-I560T-R	GCCAGTGCGCGGTGAGCGCAAAGGT
KCNH2-A561V-F	CTTTGCGCTCATCGTGCACTGGCTAGCC
KCNH2-A561V-R	GGCTAGCCAGTGCACGATGAGCGCAAAG

Table S3: GenBank accession numbers for *KCNH2* proteins

Species	GenBank Accession number
Human	NP_000229
Chimp	XP_001137384
Macaca	XP_002808416
Rat	NP_446401
Canine	NP_001003145
Bovine	NP_001092571
Chicken	XP_003640714
Zebrafish	NP_001036187

III. SUPPLEMENTAL FIGURES:

Supplemental figure S1: Twelve-lead ECG of Japanese SQTS patients

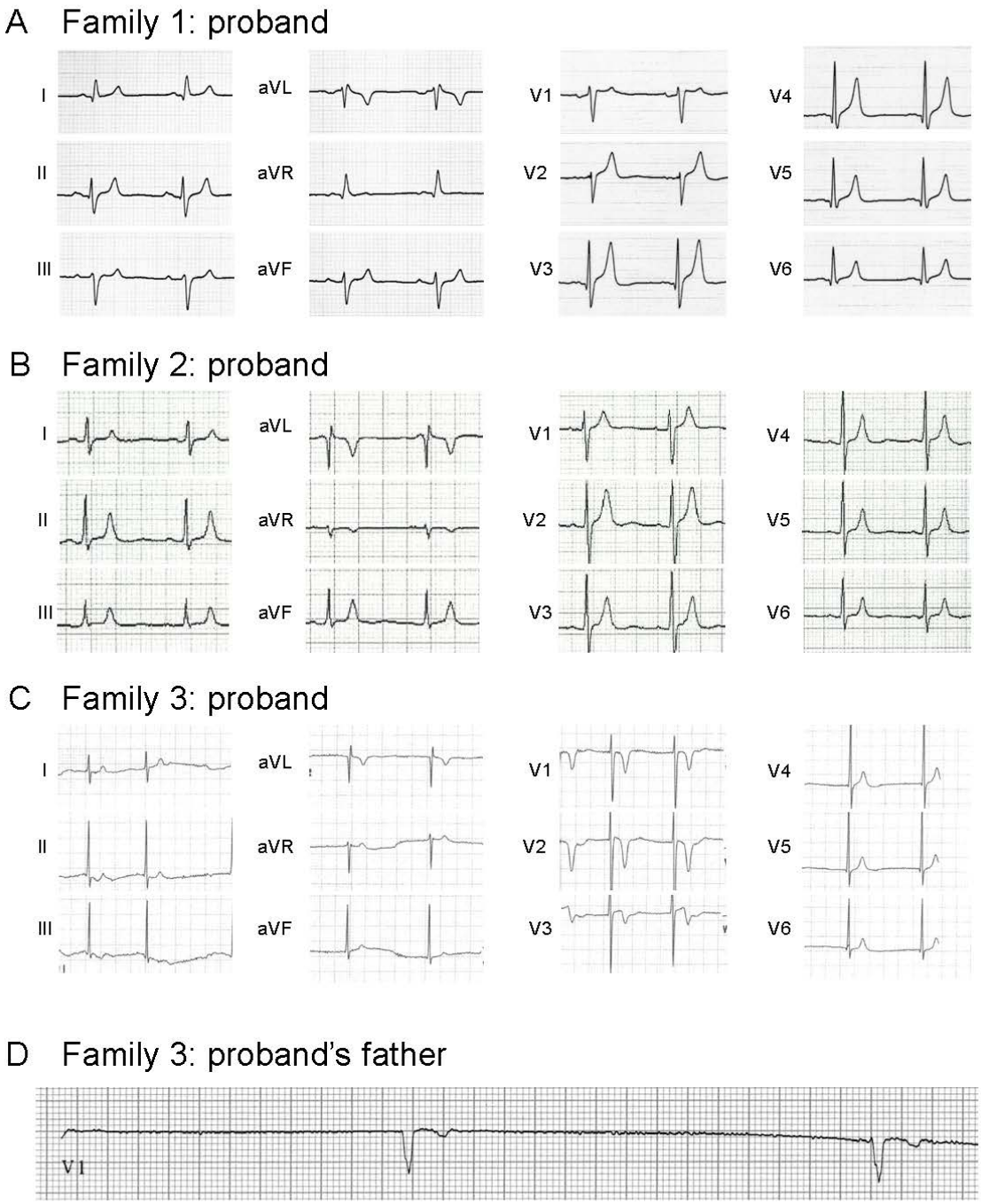

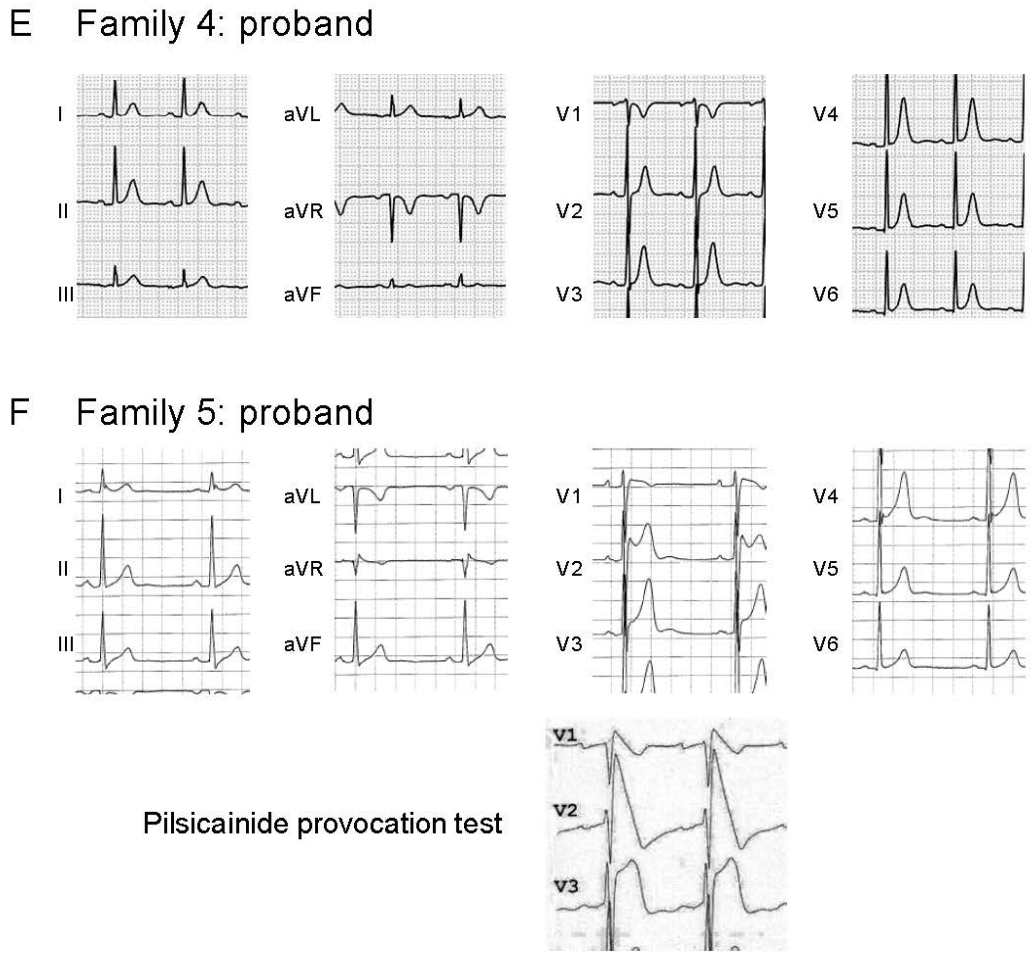

Figure S1. Twelve-lead ECGs of Japanese SQTS patients.

(A) The proband of family 1, carrying *KCNH2*-I560T, displayed short QTc of 319 ms with paroxysmal AF and atrial flutter.

(B) The proband of family 2, a VF survivor carrying *KCNH2*-T618I, showed short QTc of 322 ms.

(C) The proband of family 3, carrying *KCNQ1*-V141M, exhibited SSS and short QTc of 280 ms.

(D) Father of the family 3 proband had chronic AF with bradycardia with QTc of 375 ms, despite carrying the *KCNQ1* mutation V141M identical to the proband.

(E) The proband of family 4, a VF survivor, showed short QTc of 330 ms.

(F) The proband of family 5 displayed short QTc of 340 ms. Saddle-back ST elevation on the right precordial leads was converted to coved-type ST elevation characteristic for Brugada syndrome during the pilsicainide provocation test.

Supplemental figure S2: Simulated current traces of *KCNH2*-I560T

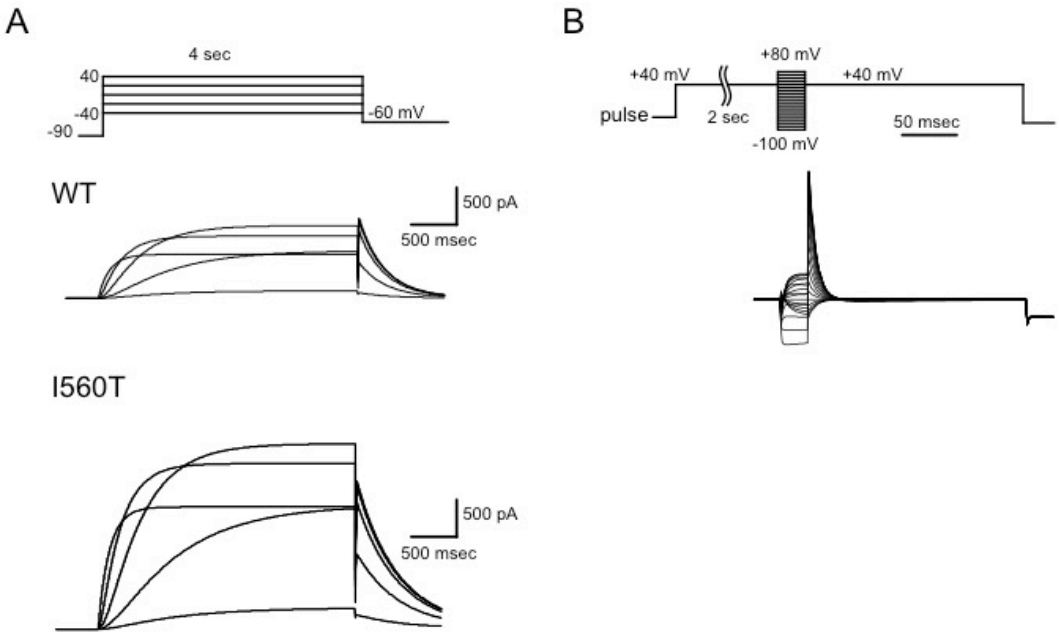

Figure S2: Simulated current traces of *KCNH2*-I560T

(A) I_{Kr} current traces of WT and *KCNH2*-I560T obtained from modified Markov I_{Kr} model.

(B) Representative traces of I560T obtained from simulated multi-pulse protocol to determine channel availability.

IV. REFERENCES

[1] Priori SG, Wilde AA, Horie M, Cho Y, Behr ER, Berul C, et al. HRS/EHRA/APHRS expert consensus statement on the diagnosis and management of patients with inherited primary arrhythmia syndromes: document endorsed by HRS, EHRA, and APHRS in May 2013 and by ACCF, AHA, PACES, and AEPC in June 2013. Heart Rhythm. 2013;10:1932-63.

[2] Gollob MH, Redpath CJ, Roberts JD. The short QT syndrome: proposed diagnostic criteria. J Am Coll Cardiol. 2011;57:802-12.

[3] Antzelevitch C, Pollevick GD, Cordeiro JM, Casis O, Sanguinetti MC, Aizawa Y, et al. Loss-of-function mutations in the cardiac calcium channel underlie a new clinical entity characterized by ST-segment elevation, short QT intervals, and sudden cardiac death. Circulation. 2007;115:442-9.

[4] Templin C, Ghadri JR, Rougier JS, Baumer A, Kaplan V, Albesa M, et al. Identification of a novel loss-of-function calcium channel gene mutation in short QT syndrome (SQTS6). Eur Heart J. 2011;32:1077-88.

[5] Mazzanti A, Kanthan A, Monteforte N, Memmi M, Bloise R, Novelli V, et al. Novel insight into the natural history of short QT syndrome. J Am Coll Cardiol. 2014;63:1300-8.

[6] Giustetto C, Schimpf R, Mazzanti A, Scrocco C, Maury P, Anttonen O, et al. Long-term follow-up of patients with short QT syndrome. J Am Coll Cardiol. 2011;58:587-95.

[7] Villafane J, Atallah J, Gollob MH, Maury P, Wolpert C, Gebauer R, et al. Long-term follow-up of a pediatric cohort with short QT syndrome. J Am Coll Cardiol. 2013;61:1183-91.

[8] Villafane J, Fischbach P, Gebauer R. Short QT syndrome manifesting with neonatal atrial fibrillation and bradycardia. Cardiology. 2014;128:236-40.

[9] Sun Y, Quan XQ, Fromme S, Cox RH, Zhang P, Zhang L, et al. A novel mutation in the KCNH2 gene associated with short QT syndrome. J Mol Cell Cardiol. 2011;50:433-41.

[10] Hong K, Piper DR, Diaz-Valdecantos A, Brugada J, Oliva A, Burashnikov E, et al. De novo KCNQ1 mutation responsible for atrial fibrillation and short QT syndrome in utero. Cardiovasc Res. 2005;68:433-40.

[11] Deo M, Ruan Y, Pandit SV, Shah K, Berenfeld O, Blaufox A, et al. KCNJ2 mutation in short QT syndrome 3 results in atrial fibrillation and ventricular proarrhythmia. Proc Natl Acad Sci U S A. 2013;110:4291-6.

[12] Hattori T, Makiyama T, Akao M, Ehara E, Ohno S, Iguchi M, et al. A novel gain-of-function KCNJ2 mutation associated with short-QT syndrome impairs inward rectification of Kir2.1 currents. Cardiovasc Res. 2012;93:666-73.

[13] Maury P, Hollington L, Duparc A, Brugada R. Short QT syndrome: Should we push the frontier forward? Heart Rhythm. 2005;2:1135-7.
[14] Itoh H, Sakaguchi T, Ashihara T, Ding WG, Nagaoka I, Oka Y, et al. A novel KCNH2 mutation as a modifier for short QT interval. Int J Cardiol. 2009;137:83-5.
[15] Hong K, Bjerregaard P, Gussak I, Brugada R. Short QT syndrome and atrial fibrillation caused by mutation in KCNH2. J Cardiovasc Electrophysiol. 2005;16:394-6.
[16] Giustetto C, Di Monte F, Wolpert C, Borggrefe M, Schimpf R, Sbragia P, et al. Short QT syndrome: clinical findings and diagnostic-therapeutic implications. Eur Heart J. 2006;27:2440-7.
[17] Gaita F, Giustetto C, Bianchi F, Wolpert C, Schimpf R, Riccardi R, et al. Short QT Syndrome: a familial cause of sudden death. Circulation. 2003;108:965-70.
[18] Redpath CJ, Green MS, Birnie DH, Gollob MH. Rapid genetic testing facilitating the diagnosis of short QT syndrome. Can J Cardiol. 2009;25:e133-5.
[19] Splawski I, Shen J, Timothy KW, Vincent GM, Lehmann MH, Keating MT. Genomic structure of three long QT syndrome genes: KVLQT1, HERG, and KCNE1. Genomics. 1998;51:86-97.
[20] Syrris P, Murray A, Carter ND, McKenna WM, Jeffery S. Mutation detection in long QT syndrome: a comprehensive set of primers and PCR conditions. J Med Genet. 2001;38:705-10.
[21] Plaster NM, Tawil R, Tristani-Firouzi M, Canun S, Bendahhou S, Tsunoda A, et al. Mutations in Kir2.1 cause the developmental and episodic electrical phenotypes of Andersen's syndrome. Cell. 2001;105:511-9.
[22] Hu D, Barajas-Martinez H, Pfeiffer R, Dezi F, Pfeiffer J, Buch T, et al. Mutations in SCN10A are responsible for a large fraction of cases of Brugada syndrome. J Am Coll Cardiol. 2014;64:66-79.
[23] Abe K, Machida T, Sumitomo N, Yamamoto H, Ohkubo K, Watanabe I, et al. Sodium channelopathy underlying familial sick sinus syndrome with early onset and predominantly male characteristics. Circ Arrhythm Electrophysiol. 2014;7:511-7.
[24] Liu H, Chatel S, Simard C, Syam N, Salle L, Probst V, et al. Molecular Genetics and Functional Anomalies in a Series of 248 Brugada Cases with 11 Mutations in the TRPM4 Channel. PLoS ONE. 2013;8:e54131.
[25] Giudicessi JR, Ye D, Tester DJ, Crotti L, Mugione A, Nesterenko VV, et al. Transient outward current (Ito) gain-of-function mutations in the KCND3-encoded Kv4.3 potassium channel and Brugada syndrome. Heart Rhythm. 2011;8:1024-32.
[26] Delpón E, Cordeiro JM, Núñez L, Thomsen PEB, Guerchicoff A, Pollevick GD, et al.

Functional effects of KCNE3 mutation and its role in the development of Brugada syndrome. Circ Arrhythmia Electrophysiol 2008;1:209-18.
[27] Ishikawa T, Takahashi N, Ohno S, Sakurada H, Nakamura K, On YK, et al. Novel SCN3B Mutation Associated With Brugada Syndrome Affects Intracellular Trafficking and Function of Nav1.5. Circ J. 2013;77:959-67.
[28] Makita N, Sloan-Brown K, Weghuis DO, Ropers HH, George AL, Jr. Genomic organization and chromosomal assignment of the human voltage-gated Na^+ channel beta 1 subunit gene (SCN1B). Genomics. 1994;23:628-34.
[29] Kagan A, Yu Z, Fishman GI, McDonald TV. The dominant negative LQT2 mutation A561V reduces wild-type HERG expression. J Biol Chem. 2000;275:11241-8.
[30] O'Hara T, Virag L, Varro A, Rudy Y. Simulation of the undiseased human cardiac ventricular action potential: model formulation and experimental validation. PLoS Comput Biol. 2011;7:e1002061.
[31] Tsuji-Wakisaka K, Akao M, Ishii TM, Ashihara T, Makiyama T, Ohno S, et al. Identification and functional characterization of KCNQ1 mutations around the exon 7-intron 7 junction affecting the splicing process. Biochim Biophys Acta. 2011;1812:1452-9.
[32] Clancy CE, Rudy Y. Cellular consequences of HERG mutations in the long QT syndrome: precursors to sudden cardiac death. Cardiovasc Res. 2001;50:301-13.
[33] Adeniran I, McPate MJ, Witchel HJ, Hancox JC, Zhang H. Increased vulnerability of human ventricle to re-entrant excitation in hERG-linked variant 1 short QT syndrome. PLoS Comput Biol. 2011;7:e1002313.
[34] Yamada KA, Kanter EM, Green KG, Saffitz JE. Transmural distribution of connexins in rodent hearts. J Cardiovasc Electrophysiol. 2004;15:710-5.
[35] Ashihara T, Namba T, Ikeda T, Ito M, Kinoshita M, Nakazawa K. Breakthrough waves during ventricular fibrillation depend on the degree of rotational anisotropy and the boundary conditions: a simulation study. J Cardiovasc Electrophysiol. 2001;12:312-22.
[36] Baynham CT, Knisley SB. Roles of line stimulation-induced virtual electrodes and action potential prolongation in arrhythmic propagation. J Cardiovasc Electrophysiol. 2001;12:256-63.
[37] Michaelsson M, Engle MA. Congenital complete heart block: an international study of the natural history. Cardiovasc Clin. 1972;4:85-101.

V. SUPPLEMENTAL VIDEOS

1. **Video S1: Arrhythmogenicity in *KCNH2*-WT**.
   We conducted a simulation of VF reentry with 2-D human ventricular cell model with biodomain endocardial sheet with absence of mutation. Spiral wave was triggered by S1-S2 cross-field stimulations, and spiral wave self-terminated. Curved thin white lines show trajectory of wave. Snapshots are in Figure 4E.

2. **Video S2: Arrhythmogenicity of spiral wave reentry in *KCNH2*-I560T**.
   We conducted a simulation of VF reentry with 2-D human ventricular cell model with biodomain endocardial sheet with I560T. Reentry was triggered by S1-S2 cross-field stimulations, and spiral wave reentry persisted after stimulation. Curved thin white lines show trajectory of spiral wave. Snapshots are in Figure 4F.